NJC

ROYAL SOCIETY OF CHEMISTRY

PAPER

View Article Online
View Journal

Cite this: DOI: 10.1039/c9nj05847h

BSA nanoparticles as controlled release carriers for isophethalaldoxime palladacycle complex; synthesis, characterization, *in vitro* evaluation, cytotoxicity and release kinetics analysis†

Kazem Karami, *[a] Nasrin Jamshidian,[a] Afsaneh Hajiaghasi[a] and Zahra Amirghofran[b]

A new oxime ligand named isophthalaldoxime (**1**) was synthesized by the addition of hydroxylamine hydrochloride to isophthalaldehyde. Then, a four nuclear palladacycle complex {$Pd_4[(N,C)(NOHCHC_6H_2$-$CHNOH)(\mu$-$Cl)_2]_2$} (**2**) was prepared and fully characterized using elemental analysis, FT-IR, and NMR spectroscopy. A desolvation method was employed for the synthesis of protein nanoparticles using bovine serum albumin (BSA). Then, complex (**2**) was loaded on the prepared nanoparticles with an optimized entrapment efficiency (EE) of 97.78% and loading capacity (LC) of 22.68%. FT-IR spectroscopy and circular dichroism (CD) were used for spectral studies. Field emission scanning electron microscopy (FESEM) and dynamic light scattering (DLS) measurement was applied for structural studies on the morphology, size, and zeta potential of BSA nanoparticles (BSA-NPs) and complex-loaded nanoparticles ((**2**)@BSA-NPs). The results showed the stability and acceptable size of nanoparticles prepared for the *in vitro* drug release experiment. Therefore, the *in vitro* release of (**2**) from BSA-NPs was studied using the dialysis bag method. In addition, the release mechanism was investigated by mathematical methods and the results showed that phase I and II of the release process followed Korsmeyer–Peppas and Higuchi models, respectively. Finally, the *in vitro* cytotoxicities of the synthesized nanoparticles, palladium complex, and complex-loaded nanoparticles were carried out against A549 human lung carcinoma and K562 human leukemia cell lines using MTT colorimetric assays.

Received 23rd November 2019,
Accepted 30th January 2020

DOI: 10.1039/c9nj05847h

rsc.li/njc

1. Introduction

Cancer is a class of disease characterized by out-of-control cell growth. Approximately 12.7 million people were diagnosed with cancer worldwide in 2008 and this number is expected to increase to 21 million by 2030.[1,2] There are over 100 different types of cancer and each is classified by the type of cell that is initially affected. Although the clinical treatment for cancer has made considerable progress with the improvement of surgical techniques, the wide application of new technologies, and clinical development of new drugs, cancer remains a complicated medical problem that has not yet been overcome and threatens human health and lives.[3]

Drug delivery is a promising approach for the biotechnologists and pharmacologists to develop a delivery system that can aid the drug to its target and maintain its availability for therapeutic action.[4] Indeed, the efficacy of most drugs is limited due to several reasons such as poor absorption, poor solubility, non-specific delivery, short circulating half-life, high toxicity, and high dosage.[5–7] An efficient approach to increase the efficacy and reduce the side-effects of anticancer drugs is to incorporate drugs with delivery systems such as nanoparticles.[8–10]

Precise diagnosis and effective drug delivery have been attracting considerable interest in cancer therapy over the past decades.[11] Researchers have recognized that nanotechnology is the best solution to overcome the aforesaid problem in developing an effective drug. The use of nanomaterials as pharmaceutical drug carriers to increase antitumor efficacy has been studied for more than 30 years. The important goals of nanotechnology are to target the drug at the site of action, to enhance bioavailability without side effects,[12] greater safety,[13] biocompatibility,[14] protecting a drug from degradation,[15] enhancing drug absorption by facilitating diffusion through epithelium and drug tissue distribution profile, and/or improving intracellular penetration and distribution.[16]

One of the most recent developments in designing drug-delivery systems has focused on protein-based nanoparticles as drug carriers due to their exceptional characteristics, such as

[a] *Department of Chemistry, Isfahan University of Technology, Isfahan 84156/83111, Iran. E-mail: karami@cc.iut.ac.ir*
[b] *Immunology Department and Autoimmune Diseases Research Center, Shiraz University of Medical Sciences, Shiraz, Iran*

† Electronic supplementary information (ESI) available. See DOI: 10.1039/c9nj05847h

extraordinary adsorption capacity, low toxicity, biodegradability, non-immunogenicity, stability for long duration, shelf life, amphiphilicity, and easy scale up.[17,18] In addition, they can be easily prepared under soft conditions and a large variety of protocols based on desolvation, emulsification, thermal gelation,[19] nano spray drying,[20] the NAB technology (nanoparticle albumin-bound) or self-assembly without using surfactants or toxic organic solvents in their fabrication.[21,22]

Albumin is the most abundant plasma protein and an ideal candidate for nanoparticle preparation due to its excellent properties, including extraordinary binding capacity thanks to the different drug binding sites present in its structure, easy purification, high solubility in water and pH 7.4 buffer solution (up to 40% w/v), allowing ease of delivery by injection, stability in the pH range of 4–9, and the capability of heating at 60 °C for up to 10 h without deleterious effects.[23–25]

Both bovine serum albumin (BSA) and human serum albumin (HSA) are frequently used for preparing nanoparticles of defined sizes. Due to the higher availability and lower cost of BSA compared to that of HSA, as well as the high structural and amino acid sequencing similarity (about 75%), we selected BSA for the synthesis of a nano carrier in this study. BSA is highly water soluble and binds drugs and inorganic substances non-covalently, which allows the drug to be transported in the body and be readily given up at the cell surface.[26] Also, the flexibility in conformation and presence of reactive groups (thiol, amino, and carboxylic acid groups) on BSA enable it to bind with compounds with different structures.[27] The BSA-NPs were capable of not only controlling the drug encapsulation and drug release but can also extend its circulation in the blood stream.[28]

The mechanism of drug release or pharmacokinetics has wide importance in the pharmaceutical industry in the prediction of drug release rate and helps researchers in developing effective drug formulations and more accurate dosing that saves time and money.[29,30]

Following the side effects observed for platinum-based anticancer drugs, the researchers turned to platinum analogues, *viz.*, palladium complexes. In this regard, many palladium compounds with trans, chelated, and palladacyclic structures have been prepared and their pharmacological applications have been investigated *in vitro* and *in vivo*. One of the early studies about the use of palladium complexes as anti-cancer agents were done by Graham.[31] Since the hydrolysis of palladium complexes is very fast and prevents them from reaching biological targets, researchers are now inclined to prepare palladacycle complexes containing a strong C–M σ-bond to overcome the problem of fast hydrolysis kinetics.[32]

Many palladium compounds with oxime ligands have been synthesized and their anticancer activity has been studied. In our previous studies, palladium complexes with various ligands including amines, phosphorus ylides, and oximes were provided that showed acceptable results against different cancer cell lines.[33–35] Also, given the importance of protein nanocarriers, the *in vitro* release of palladium trimer complexes with oxime ligands encapsulated in either albumin or algal cellulose nanoparticles has been reported in one of our previous works.[36]

The major goal of this study is using an albumin nanoparticle drug delivery system to control the release of the new palladium complex in a planned manner in order to have the desired therapeutic effect, protect it from degradation, and improve its function. In this way, a new complex of palladium(II) with a dioxime ligand derived from isophthalaldehyde was synthesized and characterized with spectroscopic methods. Then, BSA-NPs were prepared by the desolvation method and were used as a carrier for the synthesized complex. After that, the release mechanism was investigated by various mathematical models, including Zero-order, First-order, Higuchi, Korsmeyer–Peppas, and Hixson–Crowell.

2. Materials and methods

2.1. Materials

The starting materials and solvents were purchased from Merck and Sigma Aldrich Chemical Companies, and were used without purification. Reagent grade BSA was obtained from Sigma Aldrich Chemical Company and was applied as received. Tris(hydroxymethyl)-aminomethane (Tris) buffer was analytical reagent grade, which was obtained from Merck. Doubly distilled deionized water was used for the preparation of all solutions.

2.2. Instruments

FT-IR spectra were recorded on a FT-IR JASCO 680 spectrophotometer from 4000–400 cm^{-1} using KBr pellets. NMR spectra were recorded in DMSO-d_6 at room temperature on a Bruker spectrometer at 500 MHz (^{1}H) and 125 MHz (^{13}C), and the chemical shifts (ppm) are reported according to the internal TMS standard. Elemental analysis of carbon, hydrogen, and nitrogen was done using a CHNSO Analyzer (Elementar, Vario EL III). Nanoparticle dispersion was done with an EYELA ultrasonic cleaner (Japan). A Froilabo SW14 centrifuge (CENSW14000001, UK) was used to perform centrifugation. DenaVacuum 5005 freeze dryer (Iran) was utilized for nanoparticle preparation. Field Emission Scanning Electron Microscope (FESEM) model Quanta 450 FEG, FEI (USA) was applied for nanoparticle morphology characterization.

In vitro drug release experiments were studied in 0.13 M phosphate buffer and 100 mM NaCl at pH 7.4 inside a refrigerator incubator shaker SHER300. Each experiment was conducted in triplicate and the UV-Vis spectra were recorded on a Varian Cary 100 UV-Vis spectrophotometer employing a 1 cm path length cell. CD spectra were recorded on an AvivCircular Dichroism Spectrometer, model 215 (USA). A dynamic light scattering (DLS) apparatus (NanoQ V2.5.4.0) was applied for the size, polydispersity index (PDI), and zeta potential characterization of BSA-NPs and complex (2)@BSA-NPs.

2.3. Synthesis and methodology

2.3.1. Synthesis of oxime ligand: $NOHCHC_6H_4CHNOH$ (1). There are several methods for the preparation of oximes, including the reduction of nitro compounds,[37] oxidation of amines,[38] addition of NOCl to alkenes,[39] and addition of hydroxylamine to aldehydes or ketones.[40] According to the last method (Scheme 1), 0.16 g (4 mmol)

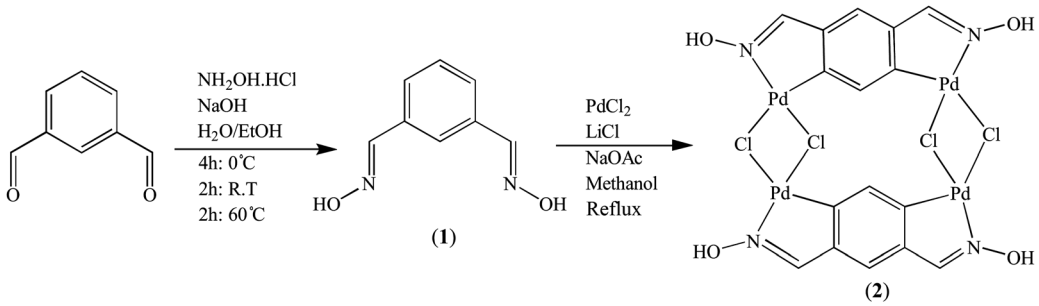

Scheme 1 Synthesis of oxime ligand (**1**) and the palladium complex (**2**).

sodium hydroxide and 0.34 g (4 mmol) hydroxylamine hydrochloride were dissolved in a solution of distilled water and ethanol (50 : 10 mL) on an ice bath and were stirred for 10 min. Then, 0.13 g (1 mmol) isophthalaldehyde was dissolved in 5 mL ethanol and was later added dropwise to the stirred solution to achieve an opaline solution. The resulting solution was stirred for 4 h at 0 °C and was then stirred at room temperature for 2 h. Eventually, the reaction mixture was refluxed for 2 h at 60 °C. The final transparent solution was left to slowly concentrate by solvent evaporation at room temperature overnight. Very fine needle crystals of (**1**) were obtained and were dissolved in acetone. The acetone solution was filtered, evaporated to a small volume, and precipitated with hexane, which was collected and dried in air to give (**1**) a white shining solid. Yield: 85%, FT-IR (KBr pellet, cm^{-1}): ν(O–H) = 3430, ν(C–$H_{aromatic}$) = 2998, ν(C=N) = 1638, ν(C=C) = 1489, δ(O–H) = 1321, ν(N–O) = 945, δ (C–H) = 680. ^{1}H-NMR (DMSO-d_6, ppm): 11.31 (s, $2H_a$), 8.14 (s, $2H_b$), 7.79 (s, $1H_c$), 7.57 (dd, $2H_d$, ^3J = 7.7 Hz, ^4J = 1.5 Hz), 7.40 (t, $1H_e$, ^3J = 7.7 Hz). ^{13}C{H} NMR (DMSO-d_6, ppm): 148.15 (C=N carbon), 133.98, 129.56, 127.56, 124.62 (aromatic carbons). Anal. calc. for $C_8H_8N_2O_2$: C, 58.53; H, 4.91; N, 17.06%. Found: C, 57.84; H, 4.05; N, 17.26%.

2.3.2. Synthesis of the palladium complex: {Pd_4[(*N*,*C*)-(NOHCHC$_6$H$_2$CHNOH)(μ-Cl)$_2$]$_2$} (2). LiCl (0.020 g, 0.48 mmol) was added to a stirred orange solution of $PdCl_2$ (0.042 g, 0.24 mmol) in MeOH (20 mL) and refluxed at 50 °C for 40 min, during which the color of the solution turned to a transparent dark red, which indicates the formation of $Li_2[PdCl_4]$. This solution was allowed to cool to 25 °C. Then, the oxime ligand (**1**) (0.020 g, 0.12 mmol) and NaOAc (0.020 g, 0.24 mmol) were added to cool down the solution, which results in a dark brown suspension immediately. This suspension was refluxed at 50 °C for 7 h. After 1 h, the color changed to light yellow and at the end of this period, a green slurry was obtained that was left to cool slowly and collected by filtration, washed with acetone and hexane, and dried in air to give a green precipitate. Yield: 79%, FT-IR (KBr pellet, cm^{-1}): ν(O–H) = 3470, ν(C–$H_{aromatic}$) = 2967, ν(C=N) = 1630, ν(C=C) = 1575, δ(O–H) = 1330, ν(N–O) = 1022, δ(C–H) = 692. ^{1}H-NMR (DMSO-d_6, ppm): 10.67 (s, $2H_a$), 8.08 (s, $2H_b$), 7.76 (s, $1H_c$), 6.95 (s, $1H_e$). ^{13}C{H} NMR (DMSO-d_6, ppm): 155.30 (C_i), 154.95 (C=N carbon), 140.77, 136.74, 122.53 (aromatic carbons). Anal. calc. for $C_{16}H_{12}N_4O_4Pd_4Cl_4$: C, 21.55; H, 1.36; N, 6.28%. Found: C, 21.03; H, 1.49; N, 6.78%.

2.3.3. Preparation of nanoparticles by the desolvation method. BSA-NPs were prepared using the well-known desolvation technique as reported before.[41] This method is a thermodynamically driven self-assembly process used for polymeric materials. Both hydrophilic and hydrophobic drugs can be encapsulated into nanoparticles employing this technique.[42,43] As a general working (Scheme 2), bovine serum albumin powder (200 mg) was dissolved in 2 mL deionized water. The pH was made to 7.2 with 0.01 M NaOH and the solution was left to stir at 500 rpm at room temperature (25 °C) for 10 min to equilibrate. Subsequently, by continuous dropwise addition of 8.0 mL ethanol by a syringe pump at the rate of 1.0 mL min^{-1} as a desolvating agent, an opalescent suspension was achieved, which indicates the formation of the nanoparticles (step i). Ethanol changes the tertiary structure of the protein and during the addition of ethanol to the solution, the albumin is phase separated due to its diminished water solubility.[44] Since the formed nanoparticles were not sufficiently stabilized and could consequently redissolve again after dispersion with water, cross-linking was implemented, which is the major step in the desolvation method. In this step, 37.5 μL 50% aqueous solution of glutaraldehyde (0.2 μL 50% Gta per mg of BSA)[45] was added gradually for the stabilization and cross linking of the amino moieties in lysine residues and the guanidine side chains in arginine of BSA *via* a condensation reaction with the aldehyde group (step ii). The mixture was maintained under stirring condition for 12 h.

2.3.4. Purification of the nanoparticles. In order to eliminate the non-desolvated albumin, the excess cross-linking agent, and organic solvent, the resulting nanoparticles were purified by three successive centrifugations (16 000 rpm, 20 min). The first centrifugation supernatant was used for the determination of non-desolvated albumin. After that, between each centrifugation, the supernatant solution was thrown away and the pellets were washed with the original volume of deionized water (step iii). Then, the redispersion step in deionized water (20 mL) was performed in an ultrasonic bath for 30 minutes (step iv). The product was dried in a freeze dryer with a cycle of 24 h at the shelf temperature of −55 °C and then incubated at 4 °C in the dark (step v). Average particle sizes were measured by scanning electron microscopy (SEM) and dynamic light scattering (DLS). The samples were dispersed in distilled water for DLS analyses.

2.3.5. Loading of the palladium complex onto BSA-NPs. The BSA nanoparticles were loaded with the complex (**2**) and

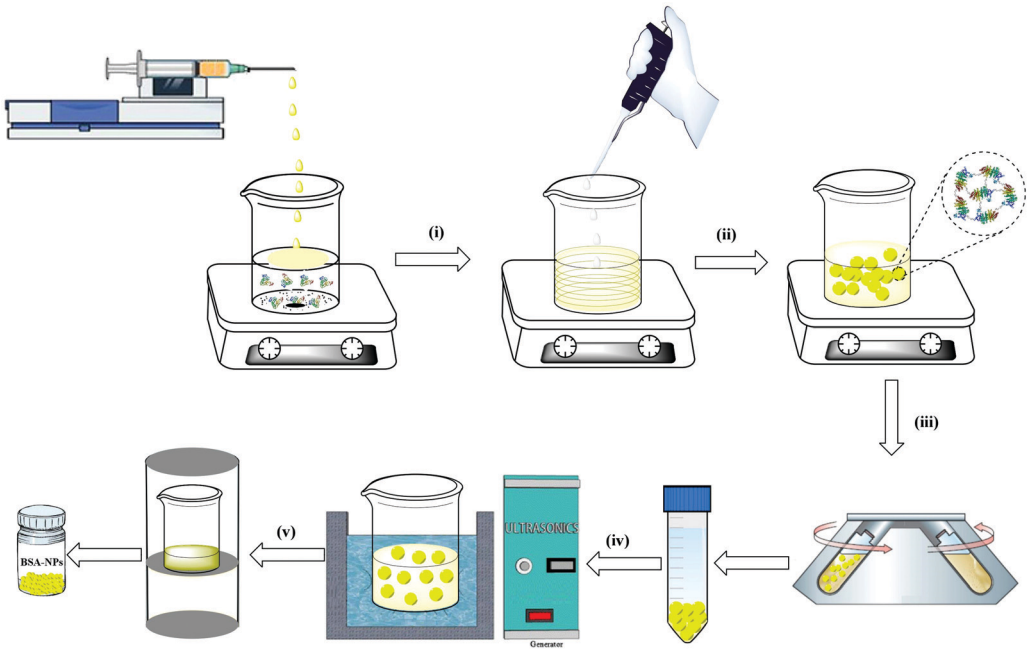

Scheme 2 Preparation and purification of the nanoparticles by the desolvation method.

were checked for the loading efficiency. The loading process was done by the preparation of nanoparticle solutions by dissolving 25 mg in 1 mL deionized water. Then, the volumes of 50–400 μL of complex (**2**) stock solution (2×10^{-3} M) were added to the nanoparticle solutions, the final volume was adjusted with deionized water to 2 mL, and was magnetically stirred for 12 h (600 rpm) at room temperature. After this, there is an adsorption equilibrium between the complex (**2**) and the surface of the nanoparticles. These suspensions were transmitted to polypropylene centrifuge tubes and centrifuged at 12 000 rpm for 20 min. The supernatants were separated and their absorbance was measured using an ultraviolet spectrophotometer to determine the loading efficiency.

2.3.6. *"In vitro"* drug release experiment. Complex (**2**)@BSA-NPs was evaluated for *in vitro* release of the drug from the protein nanoparticles by using a dialysis membrane. For this purpose, 10 mg complex (**2**)@BSA-NPs was taken and dispersed in 2 mL phosphate buffer (0.13 M) solution. The dialysis bags with molecular weight cutoff 12 kDa were plunged in double-distilled water for 12 h at room temperature before use. Then, complex (**2**)@BSA-NPs suspension (10 mg/2 mL) was poured into it and suspended in thick glass round storage bottles of borosilicate Pyrex glass with blue GL45 screw cap containing 40 mL of the receiving phase (phosphate buffer pH 7.4). The dialysis system was placed in an incubator shaker maintained at 37 °C and 170 rpm for 48 h under constant floating and stirring conditions during the experiment. At predefined time intervals, 2 mL of the release medium was removed and replaced with equal volumes of fresh phosphate buffer solution. The amount of drug in the release medium was determined by UV-Vis spectrophotometry at 303 nm and averaged from three independent experiments. The obtained release percentage was plotted against time.

2.4. Cytotoxicity assessment

The cytotoxic effects of complex (**2**), BSA-NPs, and complex (**2**)@BSA-NPs on A549 human lung carcinoma and K562 human leukemia cell lines were assessed using MTT [3-(4,5-dimethylthiazol-2-yl)-2,5-diphenyltetrazolium bromide] colorimetric assay. A predetermined number of A549 cells (7000 cells per well) and K562 (15 000 cells per well) in 96-well culture plates was seeded in triplicate and then, 10 μL of the compounds at final concentrations of 0.01 to 200 μg mL^{-1} was added. The cells were incubated at 37 °C in a humidified CO_2 incubator for 48 h and then, 10 mL of the MTT solution (5 mg mL^{-1}, Sigma) was added to each well. After 4 h incubation at the same conditions, the supernatant was removed and 150 mL dimethyl sulfoxide (DMSO) was added. After that, the optical density (OD) was detected at 570 nm with a reference wavelength of 630 nm on a microplate reader (BioTek, USA). As the negative control, the solvent (DMSO) at concentrations equal to that in the test wells was used. To determine the percentage of cell growth inhibition, the following formula was used: Inhibition (%) = 100 − [(OD of compounds/OD of negative control) × 100]. The IC_{50} (half maximal inhibitory concentration) value of different compounds was calculated using the Curve Expert software.

3. Results and discussion

3.1. Spectral characterization of the ligand and the palladium complex

FT-IR spectrum of ligand (**1**) (Fig. 1) clearly shows the absence of aldehyde C═O band (observed at 1696 cm^{-1} in the initial aldehyde spectrum) and the appearance of oxime C═N band at 1638 cm^{-1}. Also, the absorption bands due to OH stretching, OH deformation, and N–O stretching vibrations were observed at 3430, 1321, and 1083 cm^{-1}, respectively, all of which are in

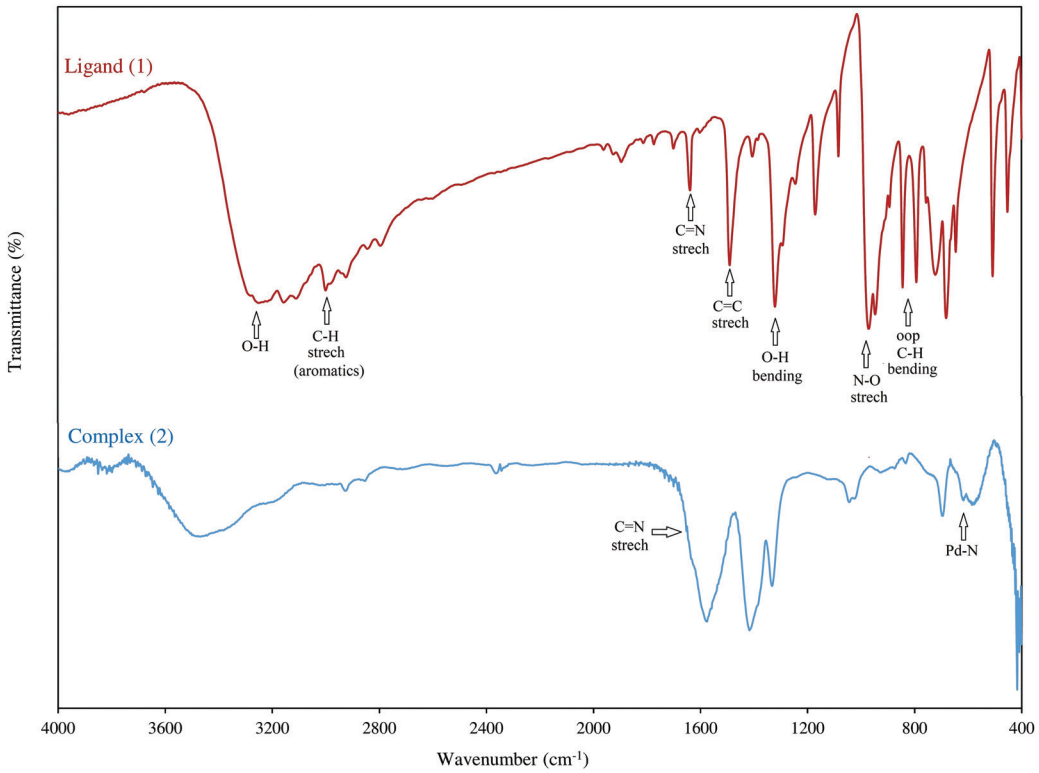

Fig. 1 Merged FT-IR spectra of the ligand (red) and the complex (blue) using KBr pellet.

accord with the previously reported oxime derivatives.[46,47] The C═N oxime stretch decreased from 1638 cm^{-1} in the free ligand to 1630 cm^{-1} in complex (**2**), which indicates that the nitrogen atoms of the C═N groups participate in the complex formation. Another important band in the FT-IR spectrum of complex (**2**) appeared at 617 cm^{-1} due to Pd–N stretching vibration.

In the ^{1}H-NMR spectrum of ligand (**1**) (Fig. S1, ESI†), the peaks corresponding protons of N–OH, N═CH, and internal aromatic C–H between two oxime groups appeared as singlets at 11.31, 8.14, and 7.79 ppm, respectively. In the ^{1}H-NMR spectrum of complex (**2**) (Fig. S2, ESI†), these peaks shifted to lower chemical shifts (10.67, 8.08, and 7.76 ppm, respectively), indicating the shielding of these protons after complex formation. The C–H protons in the ortho position of the oxime groups were in resonance as doublet of doublets at 7.57 with ^3J = 7.7 Hz and ^4J = 1.5 Hz. In the ^{1}H-NMR spectrum of complex (**2**), these protons do not appear, which is consistent with Pd(II) coordination in the proposed structure. Finally, the C–H proton in the meta position of the oxime groups was observed as a triplet at 7.40 with ^3J = 7.7 Hz. This peak appeared as a singlet at 6.95 ppm in the spectrum of complex (**2**). It confirms the removal of adjacent carbon protons due to Pd(II) coordination.

The ^{13}C{H} NMR spectrum of ligand (**1**) (Fig. S3, ESI†) shows that the carbons of C═N groups resonate at 148.15 ppm. The signals observed at 133.98, 129.56, 127.56, and 124.62 ppm are assigned to the phenyl carbon atoms ($2C_d$, C_c, $2C_f$, and C_e, respectively). In the ^{13}C{H} NMR spectrum of complex (**2**) (Fig. S4, ESI†), the signal at 155.30 ppm belongs to the palladacyclic carbon atoms and C═N carbon atom was detected at 154.95 ppm. The signals that appeared at 140.77, 136.74, and 122.53 ppm ($2C_d$, C_c and C_e, respectively) were assigned to other phenyl carbon atoms.

3.2. Nanoparticles' structural studies

3.2.1. FT-IR spectroscopy. FT-IR spectroscopy is a simple method that provides further information about the changes in the secondary structure of BSA and its characteristic bands after cross-linking with glutaraldehyde and conversion to the nano structure.[26,48] The IR spectra of pure BSA, unloaded BSA-NPs, and (**2**)@BSA-NPs are presented in Fig. 2. In the IR spectrum of proteins, there are a number of amide bands due to vibrations of the peptide moiety. As can be seen in Fig. 2, four characteristic peaks were observed for BSA, including amide I (C═O stretching vibrations) at 1649 cm^{-1}, amide II (coupling of N–H bending and C–N stretching vibrations) at 1536 cm^{-1}, side chain COO^- at 1385 cm^{-1}, and amide III (C–N stretching/N–H bending vibrations) at 1241 cm^{-1}.[49] These bands are sensitive to changes in the secondary BSA structure due to hydrogen bonding and since COO^- and N–H groups are involved in hydrogen bonding, this sensitivity is more for the amide I band.

Compared to BSA, the characteristic bands shifted to lower wavenumbers (1647, 1529, 1383, and 1232 cm^{-1}) in BSA-NPs spectrum. These slight shifts indicated no conformational changes in the secondary BSA structure due to cross linking with glutaraldehyde and nanoparticle preparation. This confirmed a chemical cross linking between tyrosine residues that could result in the overall stability of BSA NPs.

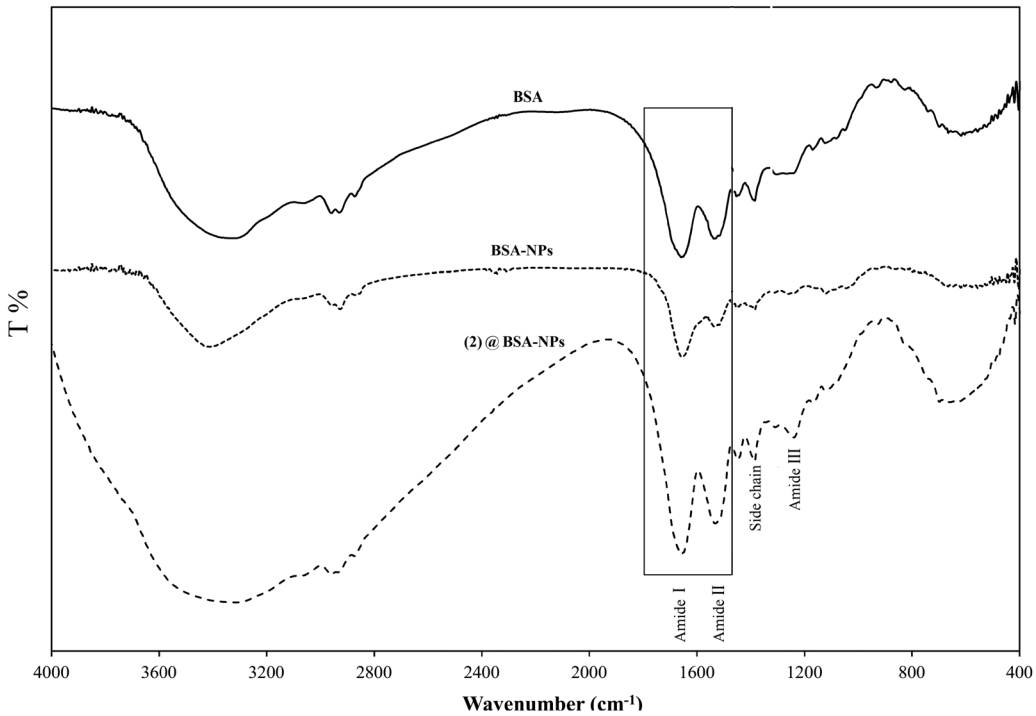

Fig. 2 Merged FT-IR spectra of pure BSA (solid line), BSA-NPs (dotted line), and (**2**)@BSA-NPs (dashed line) using KBr pellet.

The spectrum of (**2**)@BSA-NPs shows all the characteristic peaks of BSA-NPs. Also, a strong band appeared at 3300–3500 cm^{-1} and an obvious change in the O–H stretching was observed in comparison with the unloaded BSA-NPs due to oxime ligand OH group. These observations confirmed the stability of complex (**2**) in the formulation and its loading onto the synthesized nanoparticles.

3.2.2. Circular dichroism measurement. Circular dichroism spectroscopy is a powerful, fast, and sensitive photometric technique for monitoring and evaluating protein structural changes. We measured pure BSA and unloaded BSA-NPs CD spectra to examine the structural correctness and stability of this protein on nano structure conversion. As seen in Fig. 3, the CD spectrum of BSA shows two negative intense peaks near 208 and 222 nm due to n–π* and π–π* transitions of the peptide bond carbonyl group, which are protein α-helical structure characteristic feature. Compared with BSA, the characteristic CD signal did not change in the BSA-NPs spectrum. The results reveal that the α-helical predominant structure of BSA did not change after nanoparticle preparation and confirm the structural stability of the synthesized nanoparticles.[50]

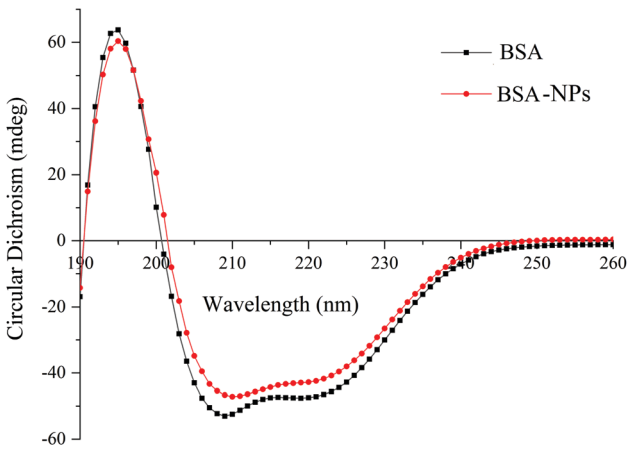

Fig. 3 Circular dichroism spectra of pure BSA (black) and desolvated BSA-NPs (red) in acetonitrile at 5×10^{-6} M concentration.

3.2.3. Morphology and size studies. The morphological investigation of the nanoparticles was conducted using FE-SEM and the obtained images are illustrated in Fig. 4a–c. As can be seen, natural protein (Fig. 4a) has a disordered structure, while for BSA-NPs (Fig. 4b), a spherical shape with a smooth surface and an average diameter of 91.77 nm was observed. Besides, complex (**2**)@BSA-NPs (Fig. 4c) were very orderly sphere-shaped with a rough surface and mean size of 97.01 nm due to palladium complex loading. It is obvious that the size of the nanoparticle support (BSA-NPs) changes, while the general morphology does not.

The obtained size of the spherical nanoparticles and palladium complex loaded nanoparticles determined by dynamic light scattering was 229 and 378 nm, respectively (Fig. 5). These values were larger than the size of 91.77 and 97.01 nm, respectively, measured by SEM due to particle constriction during dehydration. These differences are consistent with the previous literature.[8,15] The low PDI values verify their narrow size distribution.

3.2.4. Zeta potential measurements. Zeta potentiometry provide surface charge of the synthesized NPs, which can confirm their stability against aggregation. Electrostatically stabilized nanosuspensions have minimum zeta potential of ±30 mV while this value is not less than ±20 mV for sterically stabilized nanosuspensions. Based on Fig. S5 (ESI†), the zeta potential for

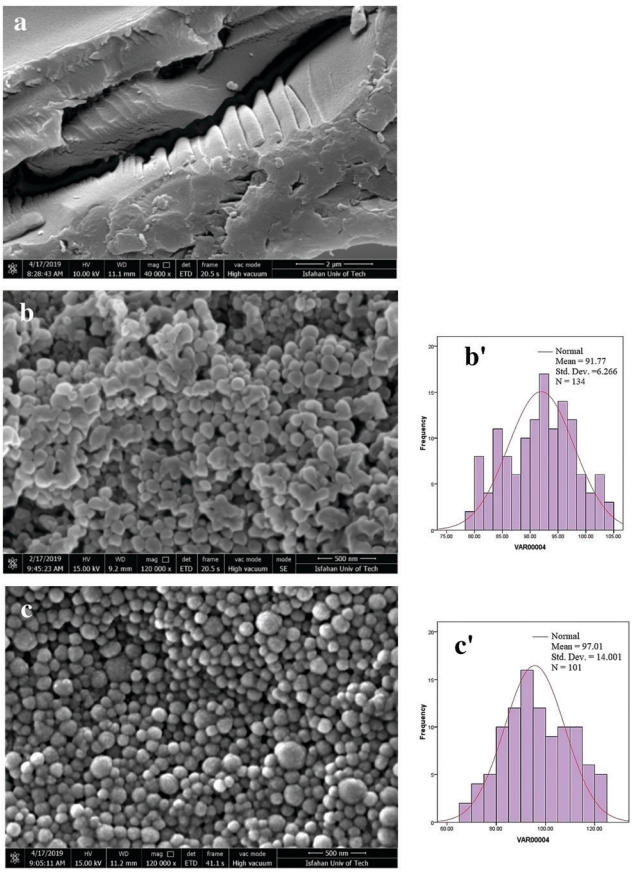

Fig. 4 SEM images and the histogram of the particle size distribution in Digimizer for pure BSA (a), BSA-NPs (b and b′), and (**2**)@BSA-NPs (c and c′).

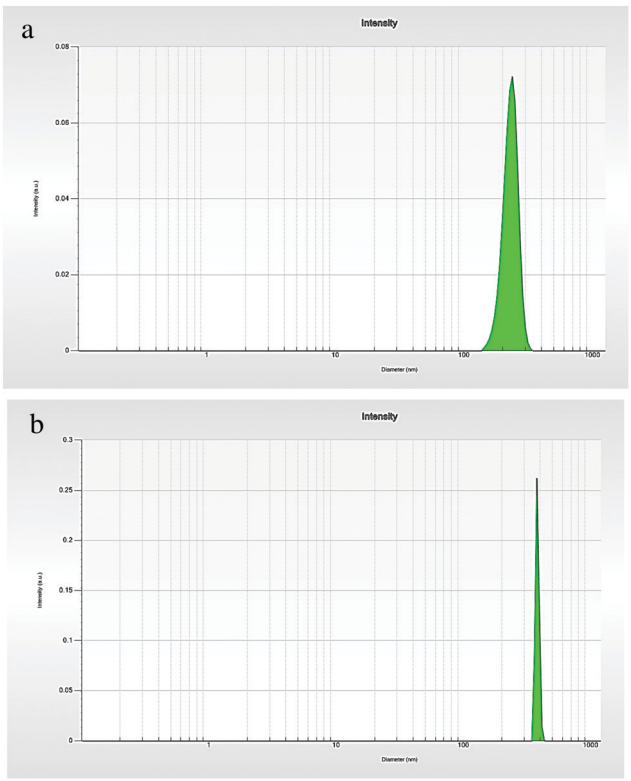

Fig. 5 Particle size distxribution of BSA-NPs (a) and (**2**)@BSA-NPs (b) determined by dynamic light scattering.

BSA-NPs was −21.5 mV, suggesting strong repulsive forces between them and electrostatic stabilization.

3.3. Drug release studies

3.3.1. Calibration curve. For the calibration curve, accurate volumes of complex (**2**) (50–400 μL) were added to the beakers containing 2 mL buffer. Thus, solutions in the concentration range of 50–250 ppm were obtained and their absorption was recorded by a UV-Vis spectrophotometer. This way, five point calibration curves were plotted in the abovementioned concentration range. As can be seen in Fig. S6 (ESI†), there is a linear relationship between the absorbance and the corresponding complex (**2**) concentration, and the absorption coefficient obtained with the determination coefficient (R^2) exceeds 0.99.

3.3.2. Calculation of the loading capacity and entrapment efficiency. BSA has internal hydrophobic cavity surfaces with natural affinities for small molecules such as metal complexes or drugs. Due to the existence of charged groups, BSA nanoparticles can bind to metal complexes non-covalently through electrostatic interactions for their effective delivery to various affected areas of the body.[51] Also, as these nanoparticles have a monolithic structure, they may be used as a matrix in which drugs can be physically entrapped.[52] The possible interactions in drug loading are hydrogen bonding and π–π stacking interactions.[53] Since the oxime functional groups in the palladium complex (**2**) structure have potential to participate in hydrogen bonds, it can be concluded that this compound binds to nanoparticles through non-covalent encapsulation.

In order to determine the loading capacity of nanoparticles and entrapment efficiency of the synthesized palladium complex, the amount of free Pd(II) complex (**2**) present in the clear supernatant after differential centrifugation was determined by an ultraviolet spectrophotometer. The amount of the loaded Pd(II) complex on the BSA-NPs was calculated by subtracting the concentration of the free Pd(II) complex in the supernatant from its initial concentration ($[\text{Pd(II) complex}]_{\text{initial}}$) and finally, the entrapment efficiency was obtained using eqn (1):

$$\text{Entrapment efficiency (\%)} = \frac{[\text{Pd(II) complex}]\ \text{initial} - [\text{Pd(II) complex}]\ \text{free}}{[\text{Pd(II) complex}]\ \text{initial}} \times 100 \quad (1)$$

where $[\text{Pd(II) complex}]_{\text{initial}}$ was varied between 56 and 280 μg mL^{-1} (50–400 μL). The loading capacity of the nanoparticles was calculated using eqn (2):

$$\text{Loading capacity (\%)} = \frac{[\text{Pd(II) complex}]\ \text{initial} - [\text{Pd(II) complex}]\ \text{free}}{[\text{BSA-NPs}]\ \text{total}} \times 100 \quad (2)$$

where $[\text{BSA-NPs}]_{\text{total}}$ is the total amount of nanoparticles recovered. As shown in Fig. S7 (ESI†), there is a dependence on the entrapment efficiency and $[\text{Pd(II) complex}]_{\text{initial}}$. The percentage

entrapment efficiency was increased along with the increase in the amount of initial Pd(II) complex, which ranged between 96.63–97.78% for 56–220 μg mL^{-1} and decreased with the increase in the amount of initial Pd(II) complex to 280 μg mL^{-1}. On the other hand, at 220 μg mL^{-1} concentration of the Pd(II) complex, the maximum amount of the metal complex was loaded onto the surface of the nanoparticle successfully. According to eqn (2), the loading capacity of the Pd(II) complex was found to be 22.68% on BSA-NPs when $[\text{Pd(II) complex}]_{\text{initial}}$ = 220 μg mL^{-1}. Actually, this parameter helps us to know the nanoparticle drug content after separation from the medium. It is clear that the nanoparticles with concentration lower than 280 μg mL^{-1} have better drug loading content. So, the optimized suspension $[\text{Pd(II) complex}]_{\text{initial}}$ = 220 μg mL^{-1} was washed by centrifugation as described above and after freezing, the product was dried in a freeze dryer with a cycle of 24 h at the shelf temperature of −40 °C and then incubated at 4 °C in the dark for the investigation of its morphology by SEM.

3.3.3. *In vitro* drug release study. The cumulative release of the synthesized Pd(II) complex is calculated using eqn (3):

$$\text{Cumulative drug release (\%)} = \frac{\text{Volume of sample withdrawn (ml)}}{\text{Bath volume (ml)}} \times P(t-1) + \text{Pt} \quad (3)$$

where Pt is the release percentage at time t and $P(t-1)$ is the release percentage before 't'. Fig. 6 shows the cumulative release profile over a period of 45 h in the pH 7.4 phosphate buffer solution (0.13 M) at 37 °C. The release profile of complex (**2**) from the BSA nanoparticles showed a single phase pattern including an initial burst release in the first 10 h, followed by a sustained release to the end of the experimental period. The initial burst release could be due to the dissolution of the adsorbed complex at or beneath the surface of the nanoparticles. After this, the cumulative release value is fixed.

For complex (**2**) loaded BSA-NPs, a biphasic release pattern is observed. In the first phase, 36.70% of release occurs within 20 h. This is because of the constant rate release of complex (**2**) into the release medium and can be related to the adsorbed Pd(II) complexes onto the nanoparticle surface, which is controlled by a diffusion process due to the electrostatic interaction. In the second phase, the release rate decreases within 45 h. Essentially, there are two possibilities for this observation. The first is increasing the diffusion pathways' length and the second is the entrapment of complex (**2**) into the BSA-NPs. Thus, the synthesized nanoparticles are capable of sustained release of complex (**2**) without burst release.

Another noticeable point is that the free complex (**2**) release amount is higher than that of the loaded one on the nanoparticles' surface, confirming their loading and decrease in the release strength. In other words, the entrapped drug in the inner core of the BSA-NPs diffuses slowly from the polymer matrix to the release medium. These observations are consistent with the various studies in which BSA-NPs has been used in drug delivery systems.[54]

3.3.4. Release mechanism study. In this section, model dependent methods were used to get further insight and to select a kinetic model for the release mechanism characterization, which can be useful in the control of the release process. The applied method is based on fitting the release data with different mathematical functions that describe the dissolution profile and compare the obtained parameters.[55–57] The equations of these functions are given below.[58,59]

$$\text{Zero-order: } f = k_0 \cdot t$$

$$\text{First-order: } f = 1 - \exp(-kt)$$

$$\text{Higuchi: } f = k_H \cdot t^{0.5}$$

$$\text{Korsmeyer–Peppas: } f = k_{KP} \cdot t^n$$

$$\text{Hixson–Crowell: } f = [1 - (1 - k_{HC} \cdot t)^3]$$

Actually, a statistical calculation was performed and the statistical indicators of the data fitting were compared for

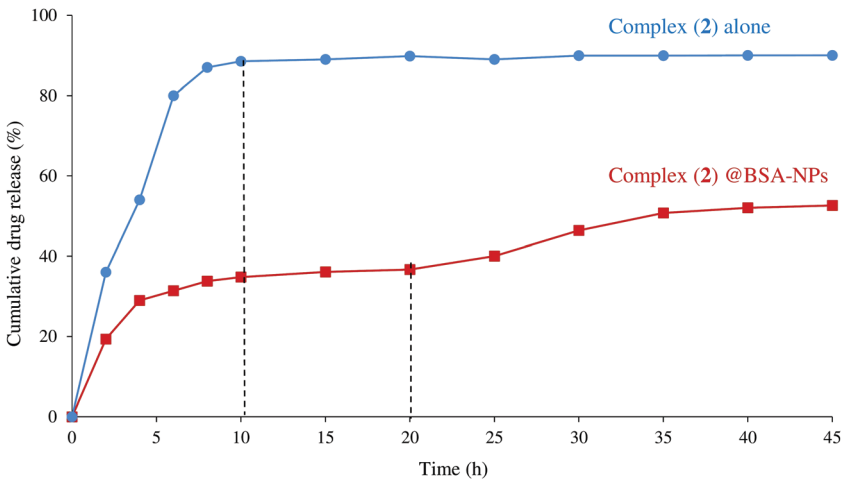

Fig. 6 *In vitro* drug release profile of free palladium complex (blue) and palladium complex loaded on BSA-NPs (red) over 48 h in phosphate buffer (pH = 7.4, 37 °C) analyzed by the dialysis method.

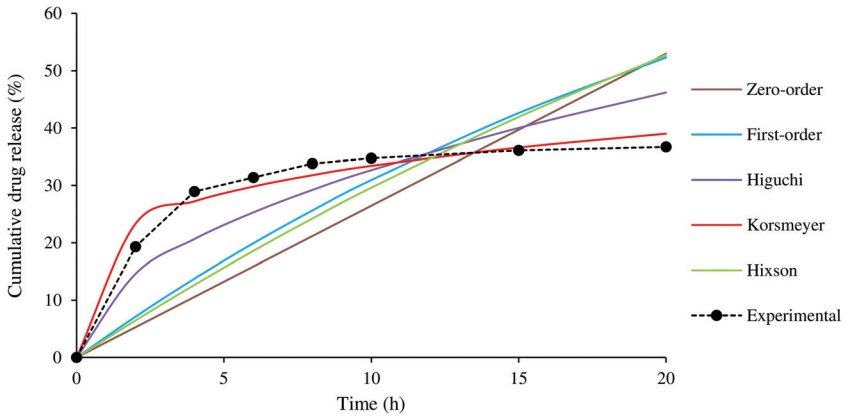

Fig. 7 Experimental (dashed line) and models predicted (colored lines) the cumulative release profile for the phase I release process.

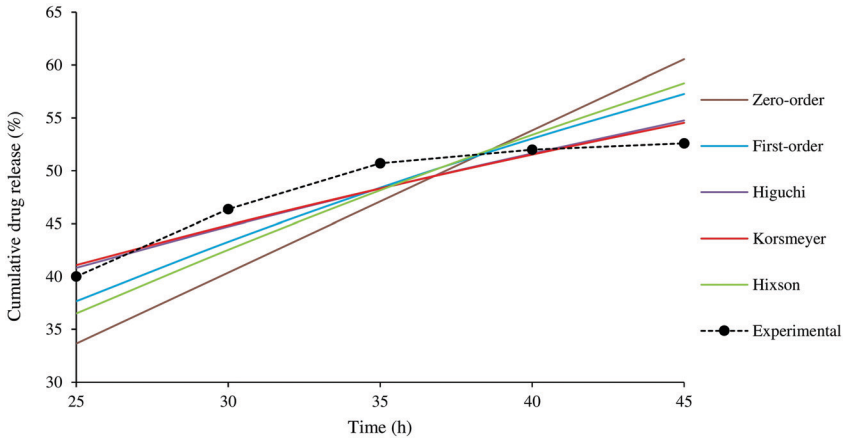

Fig. 8 Experimental (dashed line) and models predicted (colored lines) the cumulative release profile for the phase II release process.

selecting the best model. Table S1 (ESI†) shows the experimental and predicted release values for complex (**2**)@BSA-NPs that were used for drawing the cumulative drug release (%) *vs.* time (h) plots shown in Fig. 7 and 8. The results of data fitting with the mentioned equations are presented in Tables S2 and S3 (ESI†).

Several parameters have been investigated and discussed to prove the best model for drug release. The first and foremost parameter is the correlation coefficient (R^2) and according to statistical calculation rules, the best model has the nearest R^2 to 1.[60–62] Without a doubt, the important point to note is the number of parameters obtained from the models compared so that models with different numbers of parameters should be compared with the adjusted R^2.[63] As can be seen in Table 1, the obtained R^2-adj values are in the range of −0.1728 to 0.9647 and −0.0403 to 0.8659 for phase I and II release steps, respectively. So, the largest and closest values to 1 belong to the Korsmeyer–Peppas and Higuchi models for phases I and II, respectively.

The next parameter is the Akaike information criterion (AIC), which is based on the concept of entropy and shows the extent of information loss caused by the use of a statistical model. The lesser the information lost in a model, the higher the quality of the model. Thus, the model with the lowest AIC is the best.[64] The values of AIC for the release steps are given in Table 1; the lowest AIC value was obtained by fitting the data with the Korsmeyer–Peppas model for phase I and Higuchi model for phase II.

Table 1 Data of %entrapment efficiency and loading content of (**2**)@BSA-NPs

$[Pd(II)\ complex]_{initial}$	EE (%)	LC (%)
56	96.63	4.83
110	96.66	8.21
170	97.17	15.54
220	**97.78**	**22.68**
280	97.65	28.71

The important issue after determining a better kinetic model is to identify the mechanism of drug release from the surface of the nanoparticles' support. Generally, there are two release mechanism categories, including Fickian diffusion[65] and non-Fickian diffusion or anomalous transport.[66] The determination of mechanism type is possible by using the parameters obtained from the Korsmeyer–Peppas function. In this function, n is the diffusional coefficient, which is the characteristic of the release mechanism and depends on the shape of the support. For the spheres, values of n less than 0.43 indicate that the release process is controlled by Fickian diffusion, while values between

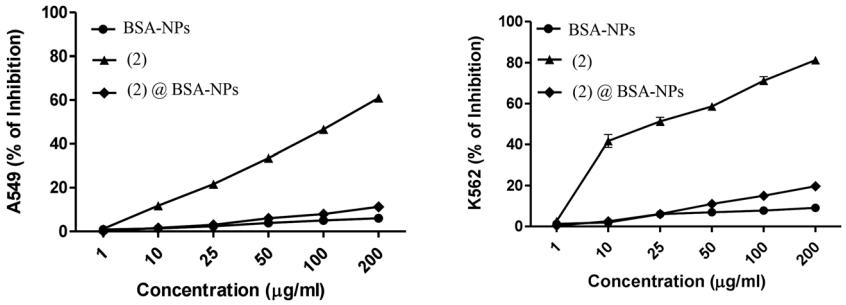

Fig. 9 Growth inhibitory effects of complex (**2**), bovine serum albumin nanoparticles (BSA-NPs), and complex (**2**) loaded NPs (complex (**2**)@BSA-NPs) on A549 and K562 tumor cell lines measured by the MTT colorimetric assay. DMSO at concentrations equal to that in the test wells was used as the negative control. Percentage of cell growth inhibition was determined according to the formula described in Section 2.4. Data represent mean ± standard deviation (SD) of two independent experiments performed at least in triplicate. The values of SD that were less than 2% are not shown.

0.43–1 are an indication of the non-Fickian diffusion mechanism.[67] In this study, the n value obtained using the Korsmeyer–Peppas equation for release phase I equals 0.223, which suggests that the release of complex (**2**) from the nanoparticles is controlled by Fickian diffusion. Besides, the release phase II data have a good fitting to the Higuchi model, which describes the drug release as a diffusion process based on the Fickian diffusion equation. According to these results, the release process of complex (**2**) from BSA-NPs is achieved by the diffusion mechanism.

3.4. *In vitro* cytotoxicity evaluation

We used the MTT colorimetric assay to evaluate the effects of various concentrations of the free complex (**2**), BSA-NPs, and complex (**2**)@BSA-NPs on the growth of two tumor cell lines including A459 and K562 cells after 48 h. As shown in Fig. 9, complex (**2**) had strong cytotoxicity against both the cell lines, especially the K562 cells, with IC_{50} values of 26.4 ± 1.6 μg mL^{-1} (K562) and 128.7 ± 4.8 μg mL^{-1} (A549). These effects were dose dependent and increased from <1% at 1 μg/m + l to 61% for A549 and 81.3% for K562 at 200 μg mL^{-1}. The BSA-NPs had no significant cytotoxic effect at the concentrations used. The effect of complex (**2**)@BSA-NPs on the cell growth was also evaluated. As seen in Fig. 9, although this complex inhibited 19.9% (K562) and 11.8% (A549) of the cell growth at the maximum concentration (200 μg mL^{-1}), in contrast to free complex (**2**), it showed a weak inhibitory effect on the cells. This finding may suggest that for observing the cytotoxic effect of complex (**2**) loaded nanoparticles, more time is needed. Cell lines such as A549 and K562 express P-glycoprotein (P-gp), which can actively pump drugs out of the cells. It is likely that complex (**2**) can inhibit the transport function of P-gp, whereas for complex (**2**)@BSA-NPs, more time is needed to overcome the multidrug resistance.

4. Conclusions

In this study, a novel oxide ligand and its corresponding palladium complex with a very interesting structure containing two Pd–C bonds on a ligand were prepared and identified by spectroscopic methods. Then, the protein nanoparticles were prepared using bovine serum albumin by desolvation method and purified. The morphology, particle size, and stability analysis studied by SEM, DLS, and CD spectroscopy indicated that the BSA-NPs were quite stable, spherical in shape, and approximately monodisperse. The synthesized nanoparticles were used as the carrier for the palladium complex. The results showed that the size of the nanoparticles did not change significantly after loading and did not exceed the acceptable range for drug delivery applications. Also, the MTT colorimetric assay was used to evaluate the effects of the prepared nanostructure support on the growth of two tumor cell lines. Finally, mathematical equations were used to investigate the mechanism of palladium complex release from the nanoparticles' surface. The results of these studies showed a two-phase mechanism for this release that followed kinetic models Korsmeyer–Peppas and Higuchi separately. The data obtained from these equations showed that the preferred mechanism in this system was non-diffusion release mechanism. Given the good results of this study, we will use other palladium compounds in future works to study their release from the surface of protein nanoparticles.

Conflicts of interest

There are no conflicts to declare.

References

1 D. Forman, C. de Martel, C. J. Lacey, I. Soerjomataram, J. Lortet-Tieulent, L. Bruni, J. Vignat, J. Ferlay, F. Bray and M. Plummer, *Vaccine*, 2012, **30**, F12.
2 C. De Martel, J. Ferlay, S. Franceschi, J. Vignat, F. Bray, D. Forman and M. Plummer, *Lancet Oncol.*, 2012, **13**, 607.
3 N. England, Improving Outcomes: A Strategy for Cancer, 2014.
4 G. Tiwari, R. Tiwari, B. Sriwastawa, L. Bhati, S. Pandey, P. Pandey and S. K. Bannerjee, *International journal of pharmaceutical investigation*, 2012, **2**, 2.
5 M. E. Ruiz, M. E. Gantner and A. Talevi, *Recent patents on anti-cancer drug discovery*, 2014, **9**, 99.
6 A. A. Manzoor, L. H. Lindner, C. D. Landon, J.-Y. Park, A. J. Simnick, M. R. Dreher, S. Das, G. Hanna, W. Park and A. Chilkoti, *Cancer Res.*, 2012, **72**, 5566.

7 G. Orive, R. M. Hernandez, A. R. G. Gascón, A. Domínguez-Gil and J. L. Pedraz, *Curr. Opin. Biotechnol.*, 2003, **14**, 659.
8 S. Bamrungsap, Z. Zhao, T. Chen, L. Wang, C. Li, T. Fu and W. Tan, *Nanomedicine*, 2012, **7**, 1253.
9 N. A. Peppas, J. Z. Hilt and J. B. Thomas, *Nanotechnology in Therapeutics: Current Technology and Applications*, Horizon Scientific Press, 2007.
10 S. Dreis, F. Rothweiler, M. Michaelis, J. Cinatl Jr, J. Kreuter and K. Langer, *Int. J. Pharm.*, 2007, **341**, 207.
11 Z. Cheng, A. Al Zaki, J. Z. Hui, V. R. Muzykantov and A. Tsourkas, *Science*, 2012, **338**, 903.
12 F. ud Din, W. Aman, I. Ullah, O. S. Qureshi, O. Mustapha, S. Shafique and A. Zeb, *Int. J. Nanomed.*, 2017, **12**, 7291.
13 F.-F. An and X.-H. Zhang, *Theranostics*, 2017, **7**, 3667.
14 S. A. Rizvi and A. M. Saleh, *Saudi Pharm. J.*, 2018, **26**, 64.
15 V. Jaishree and P. Gupta, *Indian J. Clin. Biochem.*, 2012, **27**, 214.
16 M. Millard, I. Yakavets, V. Zorin, A. Kulmukhamedova, S. Marchal and L. Bezdetnaya, *Int. J. Nanomed.*, 2017, **12**, 7993.
17 A. O. Elzoghby, W. M. Samy and N. A. Elgindy, *J. Controlled Release*, 2012, **161**, 38.
18 W. Lohcharoenkal, L. Wang, Y. C. Chen and Y. Rojanasakul, *BioMed Res. Int.*, 2014, **2014**, 180549.
19 Q. Dai, X. Zhu, S. Abbas, E. Karangwa, X. Zhang, S. Xia, B. Feng and C. Jia, *J. Agric. Food Chem.*, 2015, **63**, 4179.
20 S. H. Lee, D. Heng, W. K. Ng, H.-K. Chan and R. B. Tan, *Int. J. Pharm.*, 2011, **403**, 192.
21 S. E. Grieshaber, B. A. Paik, S. Bai, K. L. Kiick and X. Jia, *Soft Matter*, 2013, **9**, 1589.
22 S. Rohiwal, R. Satvekar, A. Tiwari, A. Raut, S. Kumbhar and S. Pawar, *Appl. Surf. Sci.*, 2015, **334**, 157.
23 M. Rahimnejad, M. Jahanshahi and G. Najafpour, *Afr. J. Biotechnol.*, 2006, **5**, 1918.
24 D. Zhao, X. Zhao, Y. Zu, J. Li, Y. Zhang, R. Jiang and Z. Zhang, *Int. J. Nanomed.*, 2010, **5**, 669.
25 E. Neumann, E. Frei, D. Funk, M. D. Becker, H.-H. Schrenk, U. Müller-Ladner and C. Fiehn, *Expert Opin. Drug Delivery*, 2010, **7**, 915.
26 E. Bronze-Uhle, B. Costa, V. Ximenes and P. Lisboa-Filho, *Nanotechnol., Sci. Appl.*, 2017, **10**, 11.
27 M. Karimi, S. Bahrami, S. B. Ravari, P. S. Zangabad, H. Mirshekari, M. Bozorgomid, S. Shahreza, M. Sori and M. R. Hamblin, *Expert Opin. Drug Delivery*, 2016, **13**, 1609.
28 M. Yu, J. Wu, J. Shi and O. C. Farokhzad, *J. Controlled Release*, 2016, **240**, 24.
29 S. Dash, P. N. Murthy, L. Nath and P. Chowdhury, *Acta Pol. Pharm.*, 2010, **67**, 217.
30 C. Aguzzi, P. Cerezo, I. Salcedo, R. Sánchez and C. Viseras, *Mater. Technol.*, 2010, **25**, 205.
31 R. D. Graham and D. R. Williams, *J. Inorg. Nucl. Chem.*, 1979, **41**, 1245.
32 A. R. Kapdi and I. J. Fairlamb, *Chem. Soc. Rev.*, 2014, **43**, 4751.
33 K. Karami, N. Jamshidian, A. Bagheri, A. Hajiaghasi, A. A. Momtazi-Borojeni, E. Abdollahi, A. Shahpiri, N. Azizi and J. Lipkowski, *J. Mol. Struct.*, 2019, **1206**, 127595.
34 K. Karami, N. Jamshidian and M. Zakariazadeh, *Appl. Organomet. Chem.*, 2019, **33**, e4728.
35 A. Jahanian-Najafabadi, M. Mirian, F. Rouhani, K. Karami, M. Hosseini Kharat and H. Sadeghi-Aliabadi, *Iran. J. Pharm. Res.*, 2019, **18**, 1323.
36 N. H. Esfahani, F. Salami, Z. Saberi, K. Karami, Z. M. Lighvan, M. Ramezani, M. Alibolandi, S. A. Farzad and T. Khayamian, *Colloids Surf., B*, 2019, **176**, 70.
37 K. Wang, X. Qian and J. Cui, *Tetrahedron*, 2009, **65**, 10377.
38 V. V. Patil, E. M. Gayakwad and G. S. Shankarling, *J. Org. Chem.*, 2016, **81**, 781.
39 M. Narendra Mallya and G. Nagendrappa, *Tetrahedron Lett.*, 2007, 155.
40 B. R. Kim, G. H. Sung, J.-J. Kim and Y.-J. Yoon, *J. Korean Chem. Soc.*, 2013, **57**, 295.
41 A. Jahanban-Esfahlan, S. Dastmalchi and S. Davaran, *Int. J. Biol. Macromol.*, 2016, **91**, 703.
42 Z. Zhao, Y. Li and M.-B. Xie, *Int. J. Mol. Sci.*, 2015, **16**, 4880.
43 A. Parodi, J. Miao, S. M. Soond, M. Rudzińska and A. A. Zamyatnin, *Biomolecules*, 2019, **9**, 218.
44 K. Langer, S. Balthasar, V. Vogel, N. Dinauer, H. Von Briesen and D. Schubert, *Int. J. Pharm.*, 2003, **257**, 169.
45 R. Sadeghi, A. Moosavi-Movahedi, Z. Emam-Jomeh, A. Kalbasi, S. Razavi, M. Karimi and J. Kokini, *J. Nanopart. Res.*, 2014, **16**, 2565.
46 B. K. Singh, U. K. Jetley, R. K. Sharma and B. S. Garg, *Spectrochim. Acta, Part A*, 2007, **68**, 63.
47 U. K. Jetley, B. K. Singh, B. S. Garg and P. Mishra, *J. Coord. Chem.*, 2007, **60**, 2243.
48 J. Grdadolnik and Y. Maréchal, *Biopolymers*, 2001, **62**, 40.
49 N. Shahgholian, G. Rajabzadeh and B. Malaekeh-Nikouei, *Int. J. Biol. Macromol.*, 2017, **104**, 788.
50 O. V. Morozova, E. R. Pavlova, D. V. Bagrov, N. A. Barinov, K. A. Prusakov, E. I. Isaeva, V. V. Podgorsky, D. V. Basmanov and D. V. Klinov, *Int. J. Nanomed.*, 2018, **13**, 6637.
51 N. M. Molino and S.-W. Wang, *Curr. Opin. Biotechnol.*, 2014, **28**, 75.
52 M. Merodio, J. M. Irache, F. Valamanesh and M. Mirshahi, *Biomaterials*, 2002, **23**, 1587.
53 M. Rai and R. Shegokar, *Metal Nanoparticles in Pharma*, Springer, 2017.
54 A. Maghsoudi, S. A. Shojaosadati and E. V. Farahani, *AAPS PharmSciTech*, 2008, **9**, 1092.
55 N. Yuksel, A. E. Kanık and T. Baykara, *Int. J. Pharm.*, 2000, **209**, 57.
56 Y. Zhang, M. Huo, J. Zhou, A. Zou, W. Li, C. Yao and S. Xie, *AAPS J.*, 2010, **12**, 263.
57 H. Lokhandwala, A. Deshpande and S. Deshpande, *International Journal of pharma and bio sciences*, 2013, **4**, 728.
58 C. Subal, Modelling of Drug release: The Higuchi equation and its application, 2006.
59 G. Singhvi and M. Singh, *International Journal of Pharmaceutical Studies and Research*, 2011, **2**, 77.
60 P. L. Bonate and J.-L. Steimer, *Pharmacokinetic-pharmacodynamic modeling and simulation*, Springer, 2011.

61 J. Bhasarkar and D. Bal, *J. Appl. Biomater. Funct. Mater.*, 2019, **17**, 1.
62 M. Barzegar-Jalali, K. Adibkia, H. Valizadeh, M. R. S. Shadbad, A. Nokhodchi, Y. Omidi, G. Mohammadi, S. H. Nezhadi and M. Hasan, *J. Pharm. Pharm. Sci.*, 2008, **11**, 167.
63 H. Motulsky, *Intuitive biostatistics: a nonmathematical guide to statistical thinking*, Oxford University Press, USA, 2014.
64 D. Anderson and K. Burnham, *Model selection and multimodel inference*, Springer-Verlag, NY, 2nd edn, 2004.
65 W. Koros and D. Punsalan, *Encyclopedia of Materials: Science and Technology*, 2001, 7305.
66 K. Ramteke, P. Dighe, A. Kharat and S. Patil, *Scholars Academic Journal of Pharmacy*, 2014, **3**, 388.
67 P. L. Ritger and N. A. Peppas, *J. Controlled Release*, 1987, **5**, 37.

